DAΦNE TECHNICAL NOTE

INFN - LNF, Accelerator Division

THE MODIFIED WIGGLER OF THE DAΦNE MAIN RINGS

A. Battisti, S. Bertolucci, B. Bolli, S. Ceravolo, M. Incurvati, F. Iungo, M. Paris,
M. Preger, P. Raimondi, C. Sanelli, F. Sardone, F. Sgamma, M. Troiani

1. Introduction

Since the first operation of DAΦNE it appeared clearly that the wigglers were a strong source of non linearities in the lattice of the collider. This was demonstrated experimentally in fall 2000 when a set of measurements was performed by creating closed orbit bumps in all the wigglers and measuring the corresponding tune shifts. Figure 1 shows the result of the measurement after subtraction of spurious effects in the other magnetic elements inside the closed orbit bump.
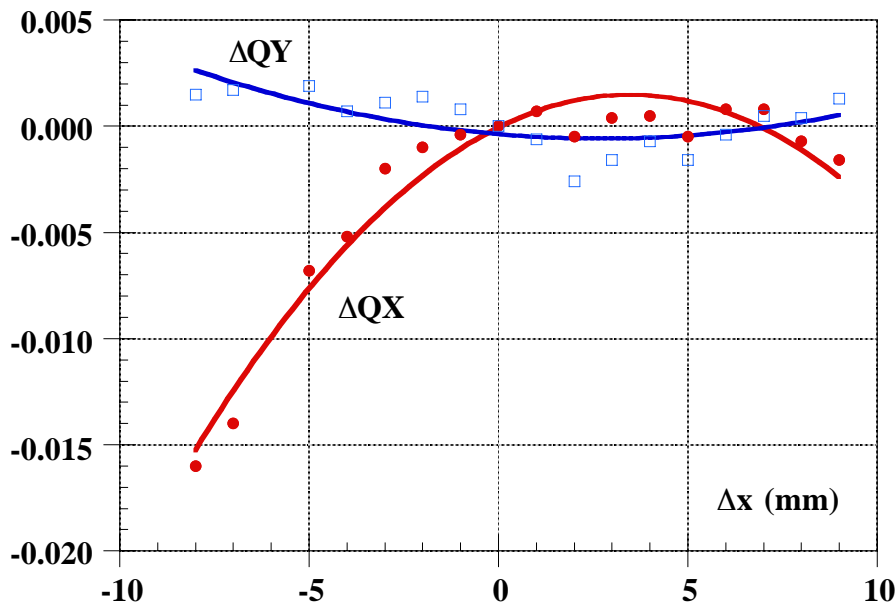
Fig. 1 - Tune shift versus beam displacement in the wiggler.

The curves in Fig. 1 are consistent with a quadratic behaviour with a curvature proportional to the beta functions in the wiggler, indicating the presence of an octupole term in the wiggler. The vertical component of the magnetic field along the wiggling trajectory of the beam can be expressed as a polynomial expansion of the field around the wiggler axis

$$B(z,x) = B(z,0) + \sum_{1}^{\infty} \frac{1}{n!} \left(\frac{\partial^n B}{\partial x^n} \right)_0 x^n$$

where z is the longitudinal coordinate along the wiggler axis, x is the horizontal position of the trajectory perpendicular to z and the derivatives are taken on the wiggler axis. The derivative of order

k of the field **along the wiggling trajectory** inside the wiggler is given by:

$$\frac{\partial^k B(z,x)}{\partial x^k} = (\frac{\partial^k B}{\partial x^k})_0 + \sum_{k+1}^{\infty} \frac{1}{(n-k)!}(\frac{\partial^n B}{\partial x^n})_0 x^{(n-k)}$$

and the effect of a (2k+2)-pole term on the beam dynamics can be expressed, in MAD notations as:

$$K_k^{MAD} = \frac{1}{B\rho} \int \frac{\partial^k B(z,x)}{\partial x^k} dz$$

The quadratic behaviour of the tune is due to a third order component of the field around the trajectory:

$$K_3^{MAD} = \frac{1}{B\rho} \int \frac{\partial^3 B(z,x)}{\partial x^3} dz = \frac{1}{B\rho} \left[\int (\frac{\partial^3 B}{\partial x^3})_0 dz + \int (\frac{\partial^4 B}{\partial x^4})_0 x(z) dz + \cdots \right]$$

The first term in the square brackets tends to vanish since the contributions from different poles have opposite signs and a third derivative of the field itself is expected to vanish due to the symmetry of the wiggler structure with respect to its simmetry axis. In the second term, on the contrary, both the fourth derivative and the wiggling trajectory change sign between one pole and the following one, so that the contributions from all poles add coherently. For this reason the quadratic behaviour of the tune has been attributed after the measurement to the combination of a fourth order component of the wiggler field with the wiggling trajectory. From a quantitative point of view, the fit of the dependence of the horizontal betatron frequency on the horizontal displacement of the beam in the wiggler and the corresponding value of the octupole constant, assuming an average value of 3 m for the horizontal betatron function in the wiggler, are:

$$\frac{\partial Q_x}{\partial x^2} = \frac{\beta_x K_3^{MAD}}{8\pi} \approx -1 \times 10^2 m^{-2} \Leftrightarrow K_3^{MAD} \approx -8 \times 10^2 m^{-3}$$

2. Measurements on the original wiggler

Since all the wigglers are operational in DAΦNE, the decision was taken to order from the same factory a ninth wiggler built on the same design and with the same materials together with 14 mm thick plates of the same rectangular shape of the poles. The goal was to machine the plates with a shape capable of reducing the higher order terms in the wiggler field and substantially increase the dynamic aperture of the ring.

The wiggler has been built by Danfysik and shipped to LNF in December 2002. As explained in [1,2], the present high precision Hall probe positioning system [3] was not available during the measurements performed on the prototype and on the wigglers presently used in the rings. However, the structure of the magnet, consisting of two C-shaped supports on each side, does not allow the measurement of a complete map in the horizontal symmetry plane with a single probe. The system was therefore modified with a T-shape support with two probes placed at a such a distance that the zones outside the range of the first probe could be always reached by the second one and the other way round. The modified support, however, was ready in fall 2003 (see Section 9) and the modification of the pole shape was realized with the single probe system.

A first measurement of the field was performed on the wiggler center pole and on one of the terminal poles at the operational currents of DAΦNE, IFP=693A in the five full poles and ITP=564A in the terminal poles. Figure 2 shows the dependence of the field at the center of the central pole as a function of the horizontal position.
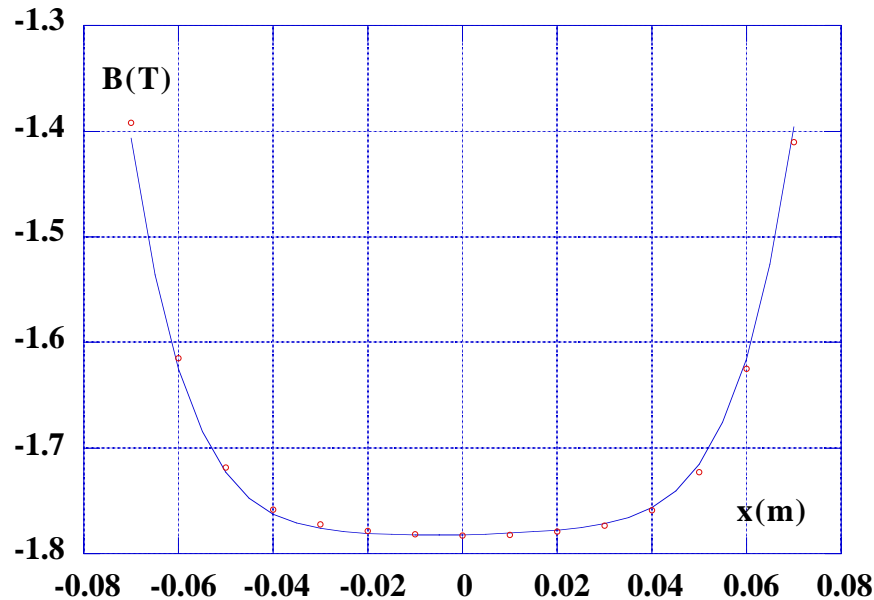
Fig. 2 - Vertical field component at magnet center versus horizontal position
dots= measured points; line=sixth order fit.

Clearly, the rapid fall-off of the field at the pole boundary (the full width of the pole is 14 cm) requires high order terms in order to fit the measurements up to 7 cm from the wiggler axis. Due to the symmetry of the magnet in the horizontal direction with respect to the wiggler axis, only even terms are expected to contribute. However, the coils are not symmetric since all connections are on the same side. We therefore allowed for a single odd term in the fit. As shown in Fig. 2, a polynomial with powers 0,1,2,6 fits reasonably the measured points at the pole center as well as at a any longitudinal position along the central and terminal poles.

$$B(z,x) = B(z,0) + \frac{\partial B}{\partial x}(z)x + \frac{1}{2}\frac{\partial^2 B}{\partial x^2}(z)x^2 + \frac{1}{720}\frac{\partial^6 B}{\partial x^6}(z)x^6$$

In order to investigate how much the field fall-off depends on the pole shape and how much on the iron saturation [1], the measurement was repeated by scaling both currents to 70% (IFP=485.1A, ITP=394.8A).

Figures 3,4,5 show the dependence of the zero, second and sixth order terms in the transverse expansion on the longitudinal position at both currents. The contribution of the first order term is negligible and the central pole is shown adjacent to the terminal pole for sake of simplicity. It can be observed in Fig. 4 that the second order term changes sign at the center of the pole at the reduced current, while it does not at full current. The fit is performed over a range from -7 cm to 7 cm with respect to the wiggler axis.
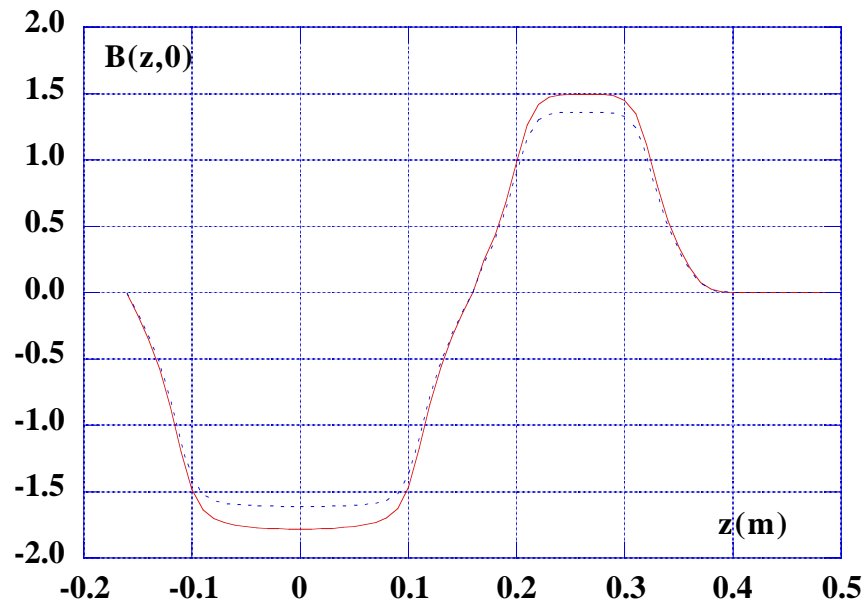
Fig. 3 - 0th order term of 6th order transverse fit versus longitudinal position.
full line = nominal current; dotted line = 70% of nominal current.
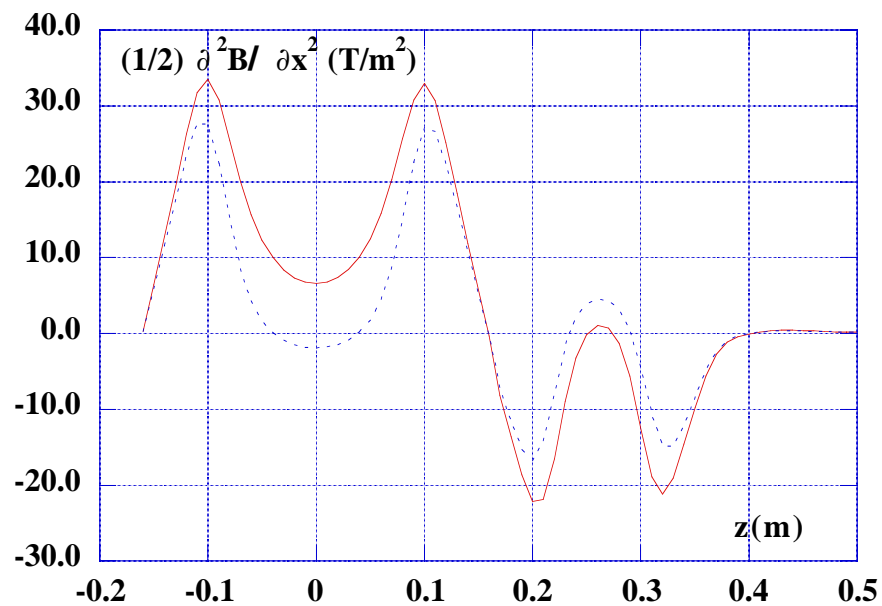
Fig. 4 - 2nd order term of 6th order transverse fit versus longitudinal position.
full line = nominal current; dotted line = 70% of nominal current.
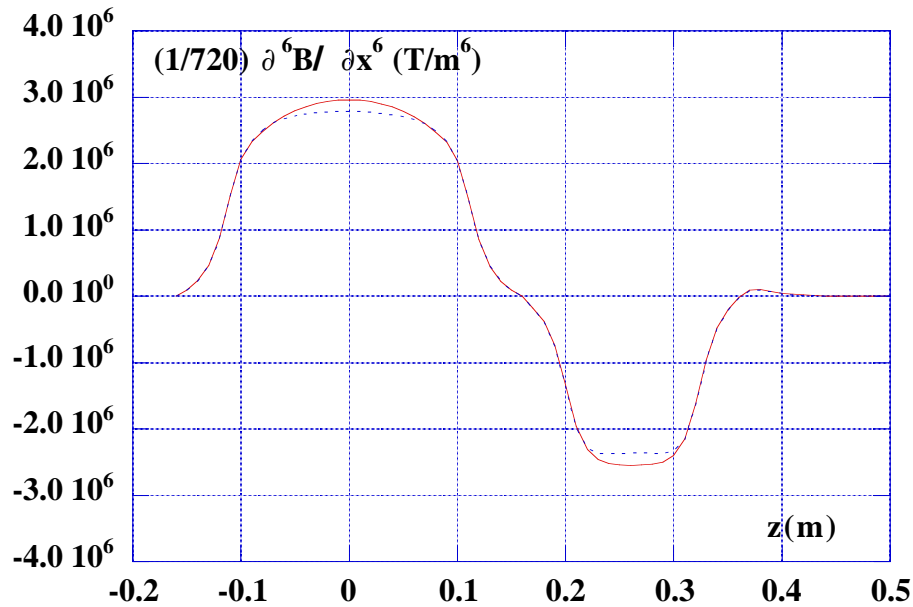
Fig. 5 - 6th order term of 6th order transverse fit versus longitudinal position.
full line = nominal current; dotted line = 70% of nominal current.

In order to check the result of the measurement of the tune shift described in Section 1, we have also performed the fit of the measured points in the central pole on a shorter range, namely from -4cm to 4 cm with a fourth order polynomial. Figs.6 and 7 show the behaviour of the second and fourth order terms of the expansion. Assuming (see following Section 10) a sinusoidal wiggle in the pole with an amplitude of ≈ 13 mm, we find a reasonable agreement between the value of K_{MAD} calculated from the fourth order term and the value obtained from the tune shift measurement.
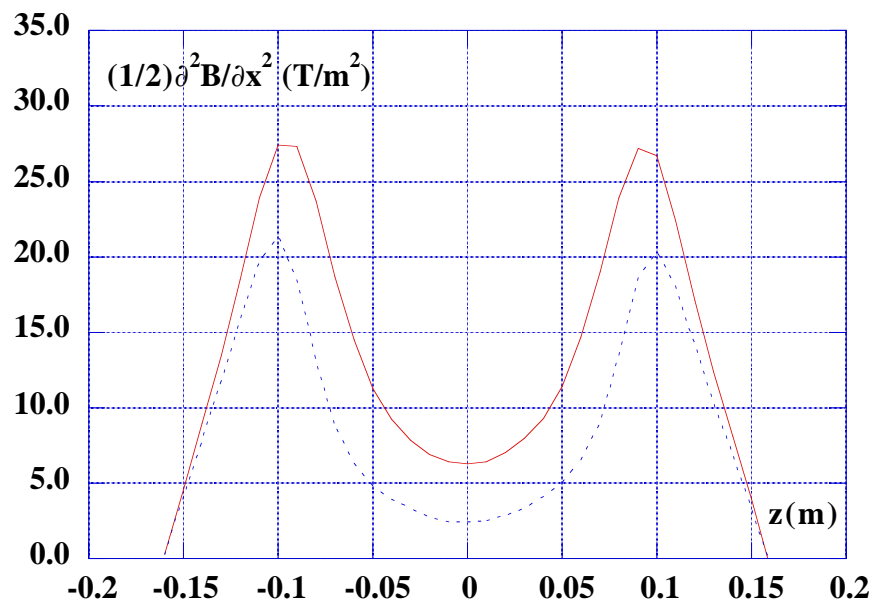
Fig. 6 - 2nd order term of 4th order polynomial fit versus longitudinal position.
full line = nominal current; dotted line = 70% of nominal current.
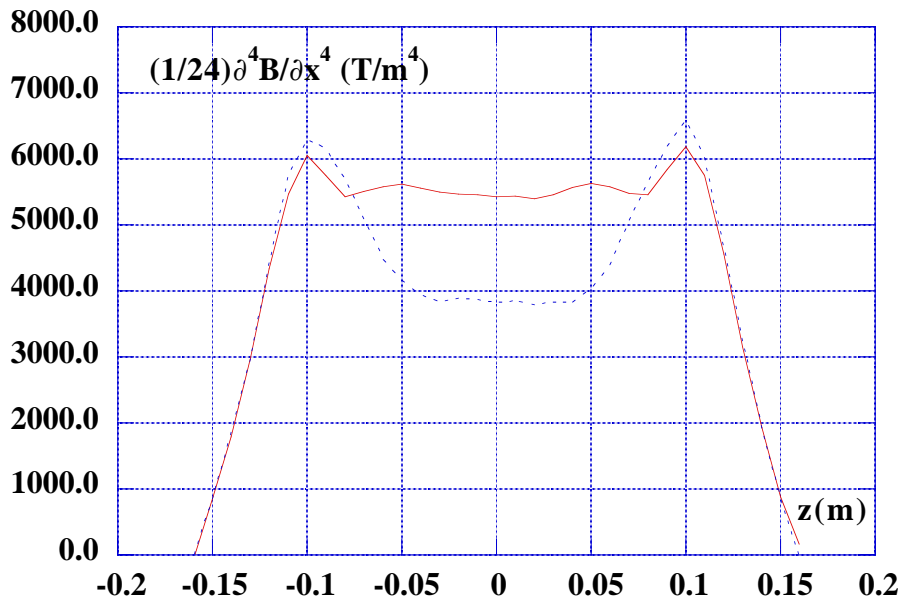
Fig. 7 - 4th order term of 4th order polynomial fit versus longitudinal position.
full line = nominal current; dotted line = 70% of nominal current.

3. Measurements on the splitted wiggler with flat poles

The following step was to split the wiggler, insert 28 mm thick separators between the two halves of each C-support and glue the flat iron plates on the poles keeping the gap at the original value of 40 mm. Figures 8,9,10 show the 0th, 2nd and 6th order components of the wide range fit respectively.
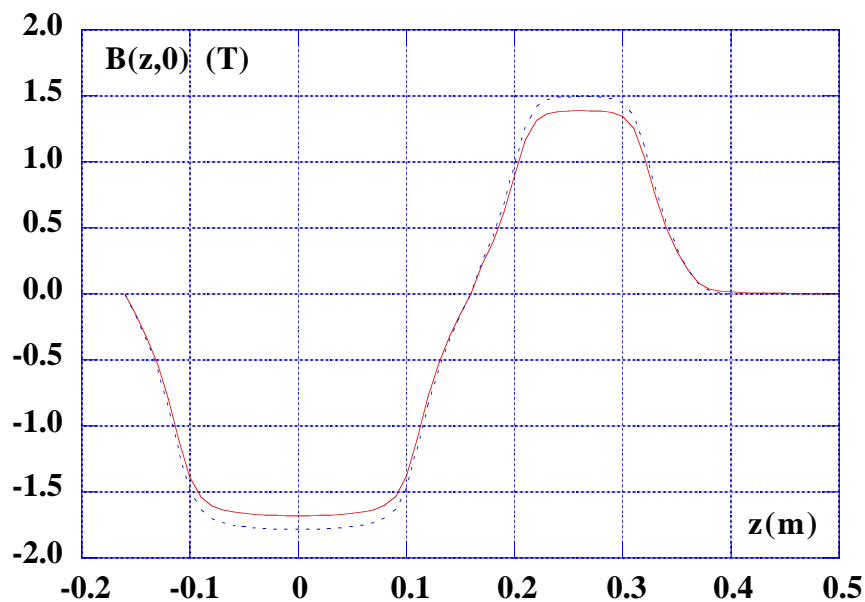
Fig. 8 - 0th order term of 6th order transverse fit versus longitudinal position.
full line = wiggler with flat glued plates; dotted line = original wiggler.
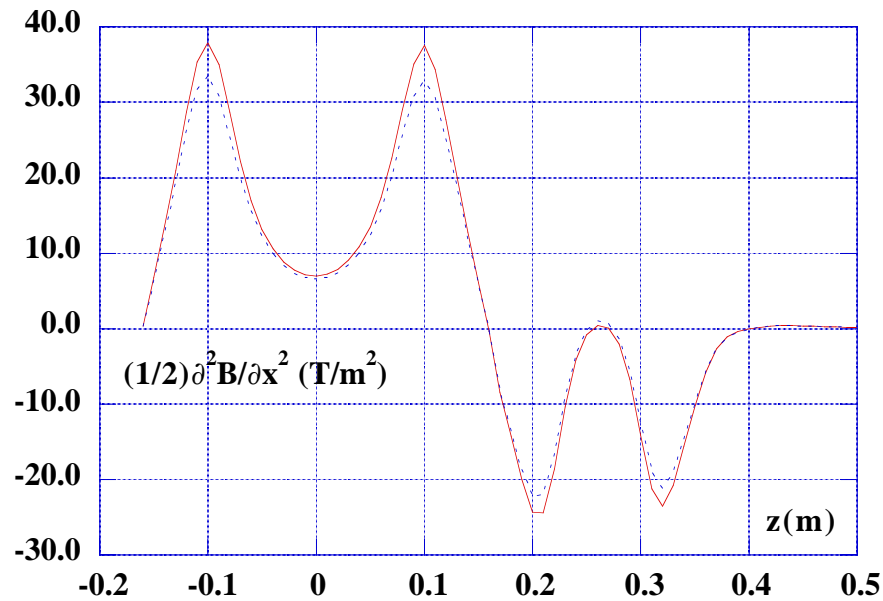
Fig. 9 - 2nd order term of 6th order transverse fit versus longitudinal position.
full line = wiggler with flat glued poles; dotted line = original wiggler.
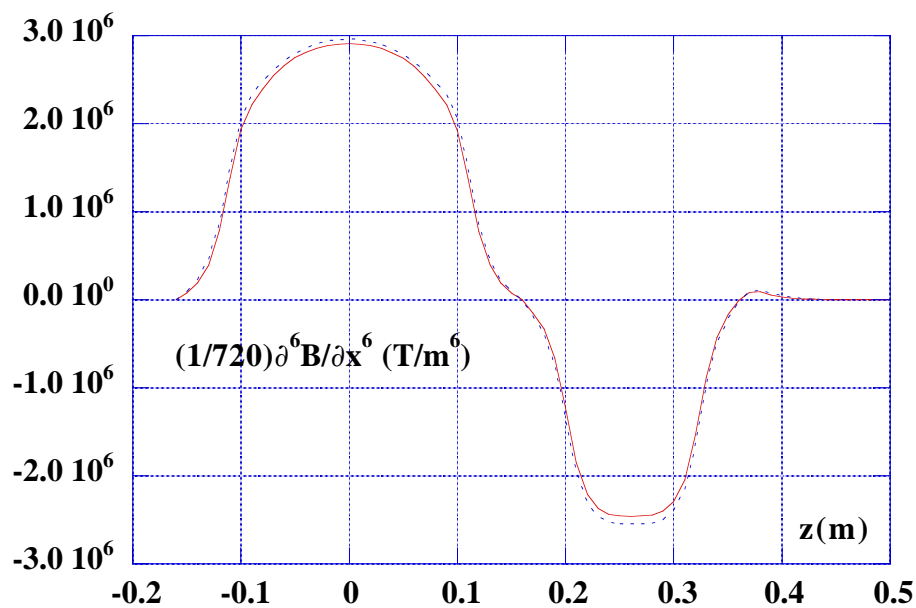
Fig. 10 - 6th order term of 6th order transverse fit versus longitudinal position.
full line = wiggler with flat glued poles; dotted line = original wiggler.

The decrease of the field due to the longer magnetic circuit is $\approx 6\%$. However, the second order term is slightly larger than in the original wiggler, while the sixth order term is smaller.

4. Modification of the pole surface

We began to modify the shape of the iron plates with the goal of flattening the variation of the field as a function of the horizontal position.

The first attempt was to increase the magnet gap where the field was higher, keeping the ratio of the measured field divided by the modified gap constant. It is clear from Fig. 2 that this cannot be applied on the whole pole width, since it would imply a >20% variation on the gap, with a strong reduction of the field on axis. We decided therefore to truncate the shaping at a distance of 6 cm, leaving the plate flat between 6 cm and 7 cm. Moreover, the curvature of the field depends on the longitudinal position along the pole, and machining the plates with the above described criterion over the whole pole surface would have been troublesome from a mechanical point of view. We took therefore the average of the curvature and obtained the pole shape shown in Fig. 11 constant over the whole wiggler length. From here on we will call this configuration as "first profile".
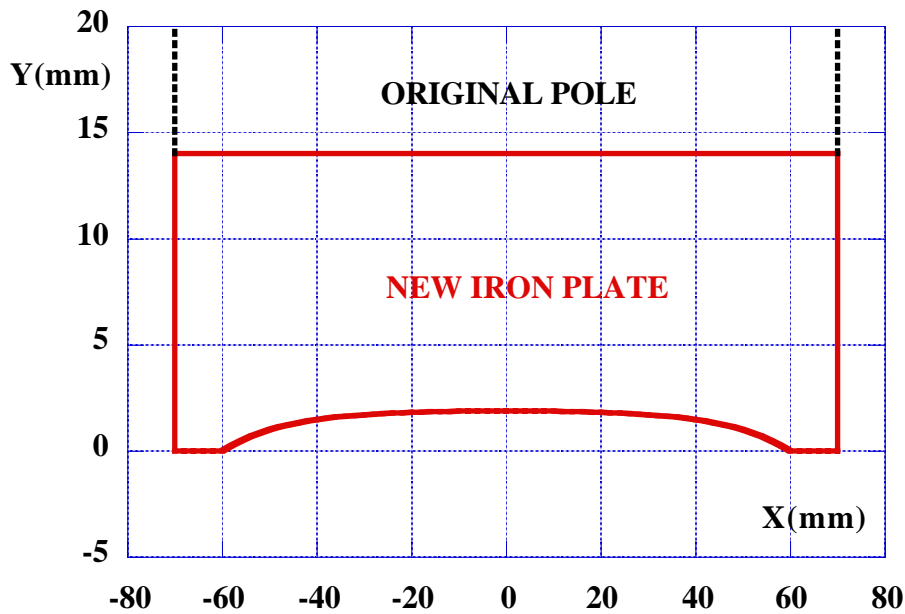
Fig. 11 - Pole shape (not in scale). The origin of the vertical scale is actually at 20 mm from the wiggler axis. The maximum gap is 43.7 mm.
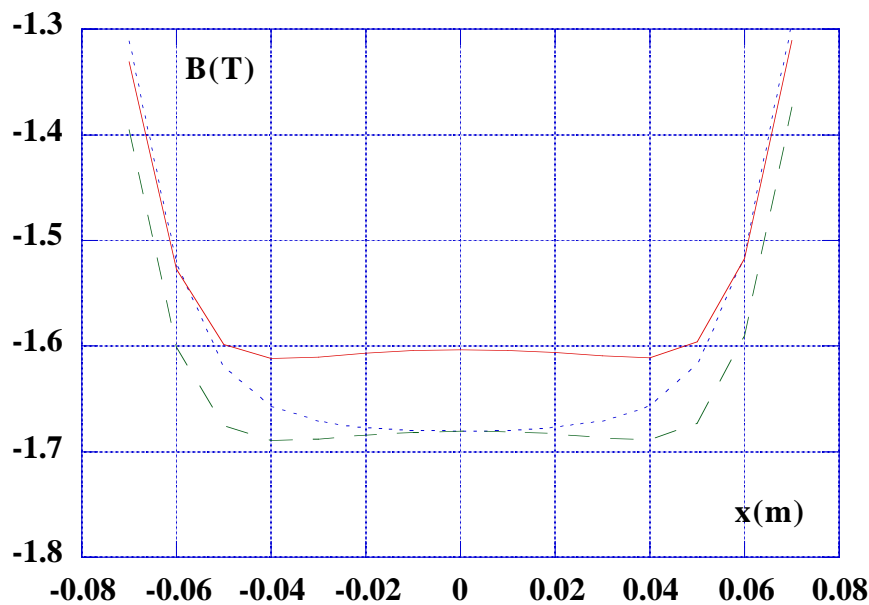
Fig. 12 - Field at magnet center versus horizontal position. Full line = first profile; dotted line = flat poles; dashed line = first profile normalized at flat pole.

The full line in Fig. 12 shows the behaviour of the field at the center of the wiggler central pole, compared to the measurement performed on the configuration with the flat plates (dotted line). The reduction in the field is ≈5%, bringing the overall reduction with respect to the original wiggler to ≈11%. The third curve (dashed line) is just the first one normalized to the value of the second on the wiggler axis, in order to better show the widening of the flat field region before the rapid drop at the pole boundary. It is also clear from Fig. 12 that the natural curvature of the field with flat poles is overcompensated at the pole center.

Due to the truncated shape of the pole the transverse fits have been performed between -6 cm and 6 cm. Figure 13 shows the measured field at the pole center and at a longitudinal distance of 10 cm, namely where the second order contribution is maximum. As can be seen from the figure, the sixth order fit defined in Section 2 still agrees with the measured points also where the curvature is overcompensated.
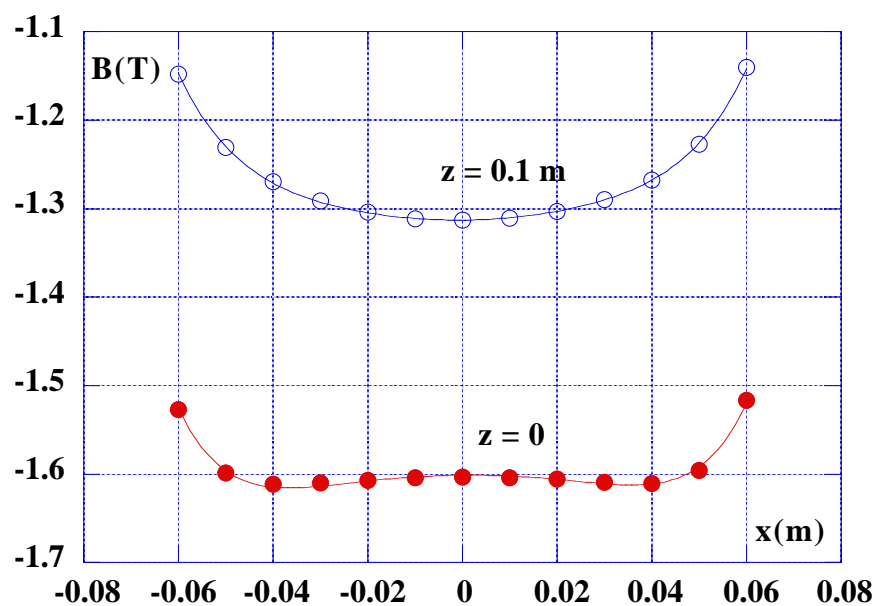
Fig. 13 -Measured field at magnet center (full dots) and at a longitudinal distance of 10 cm (empty dots) versus horizontal position. The lines through the points are the sixth order fit.

Figures 14,15,16 show the comparison between the first profile configuration and the flat poles one for the 0th, 2nd and 6th order terms of the transverse expansion as a function of the longitudinal position in the central pole. As expected, having compensated the average only, the second order term exhibits the same variation as in the case of the flat poles, but is shifted towards lower values in such a way that the integral over a single pole is strongly reduced. On the other hand, there is no significant variation on the 6th order term, although the flat field region is increased by almost 2 cm, as shown in Fig. 12. The second order term, integrated over the central pole, is reduced from 4.5 T/m to 1.9 T/m, implying a strong reduction of the linear focusing in the wiggler induced by the pole non-linearity.

In order to investigate the effect on the tune shift versus displacement of the beam in the wiggler, we have also fitted the measurements with a 4th order polynomial between -4 cm and 4 cm, as described in Section 2. The behaviour of the 4th order term is shown in Fig. 17: the reduction is more than a factor 2, indicating that the corresponding tune shift should be reduced by the same amount.
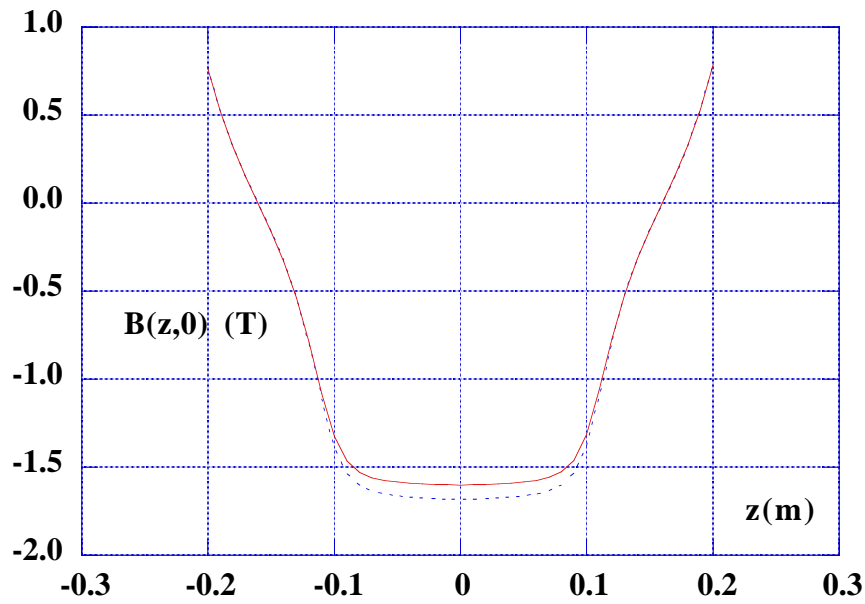
*Fig. 14 - 0th order term of 6th order transverse fit versus longitudinal position.
full line = first profile; dotted line = wiggler with flat glued plates.*
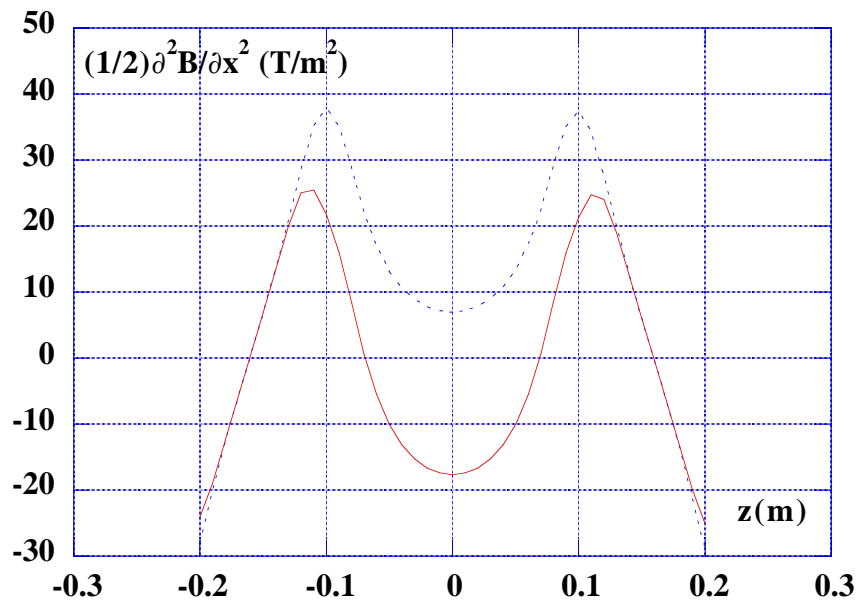
*Fig. 15 - 2nd order term of 6th order transverse fit versus longitudinal position.
full line = first profile; dotted line = wiggler with flat glued plates.*
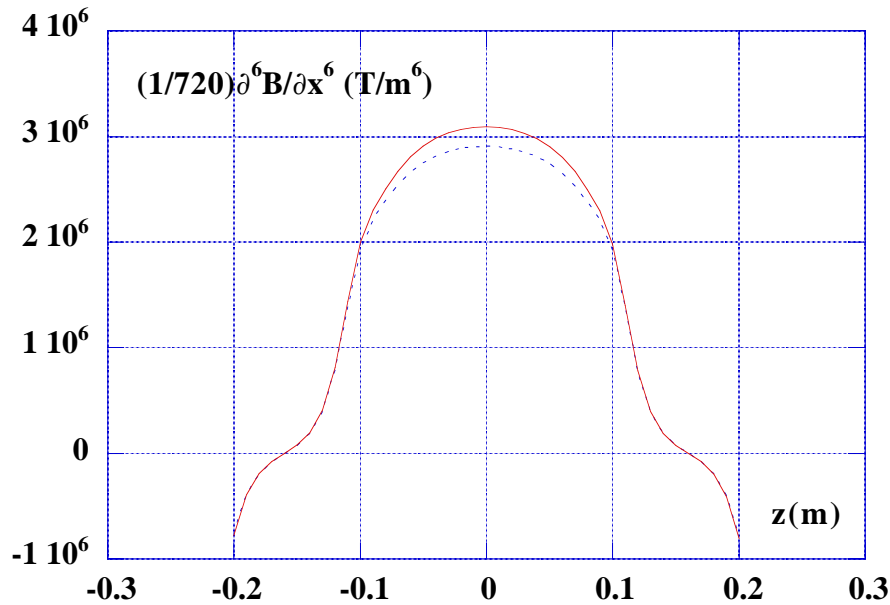
Fig. 16 - 6th order term of 6th order transverse fit versus longitudinal position.
full line = first profile; dotted line = wiggler with flat glued plates.
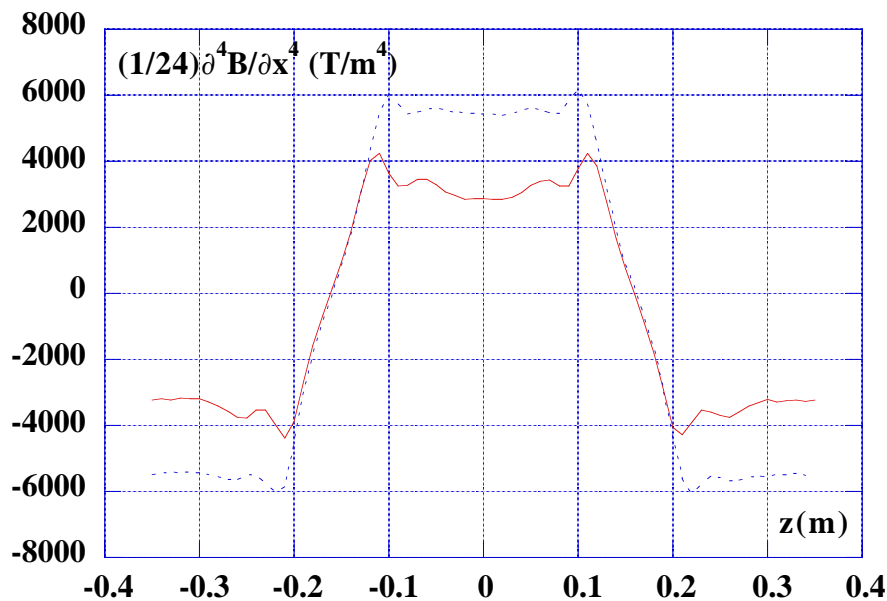
Fig. 17 - 4th order term of 4th order polynomial fit versus longitudinal position.
full line = first profile; dotted line =original wiggler

5. Modification of the pole length

In order to further reduce the effect of the non-linearity and to smoothen the peaks in the second order term of the transverse expansion shown in Fig. 15, we have modified also the length of the iron of the additional plates as a function of the horizontal distance from the wiggler axis with the criterion of making the product of the measured field integral in the first profile configuration over a straight line parallel to the wiggler axis times the iron length constant. Figure18 shows the resulting shape of the plates as seen from above. The maximum reduction of the pole length is ≈16 mm (8 mm on each side) at the pole center (on the wiggler axis). The full line indicates the end cap profile on the free surface of the plate, while the black one gives its profile (a straight line) on the surface glued on the

pole. The machined surface between the upper and lower surfaces of the plate is a family of straight lines connecting points at the same horizontal distance from the wiggler axis. This modification has been applied to the full poles, but not to the terminal ones. From here on we shall call this configuration as "second profile".
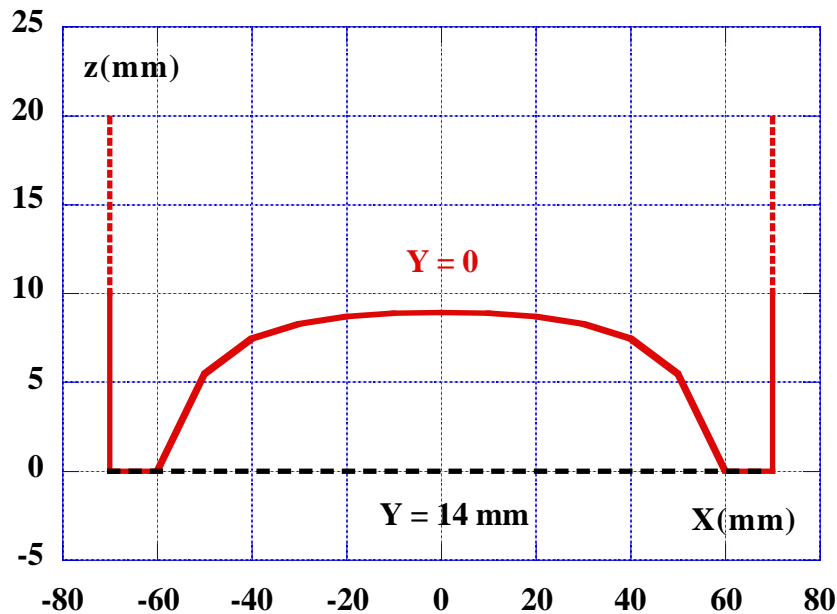
Fig. 18 - End cap of the central pole (not in scale) as seen from above

Figure 19 shows the effect on the longitudinal dependence of the second order term of the transverse expansion. The peaks are strongly smoothed and the integral of the second derivative between -16 cm and 16 cm, namely between two zero-crossings of the field, drops from 1.9 T/m to 0.7 T/m over a single pole. The sixth order term of the transverse expansion remains practically unchanged and odd terms are still negligible.
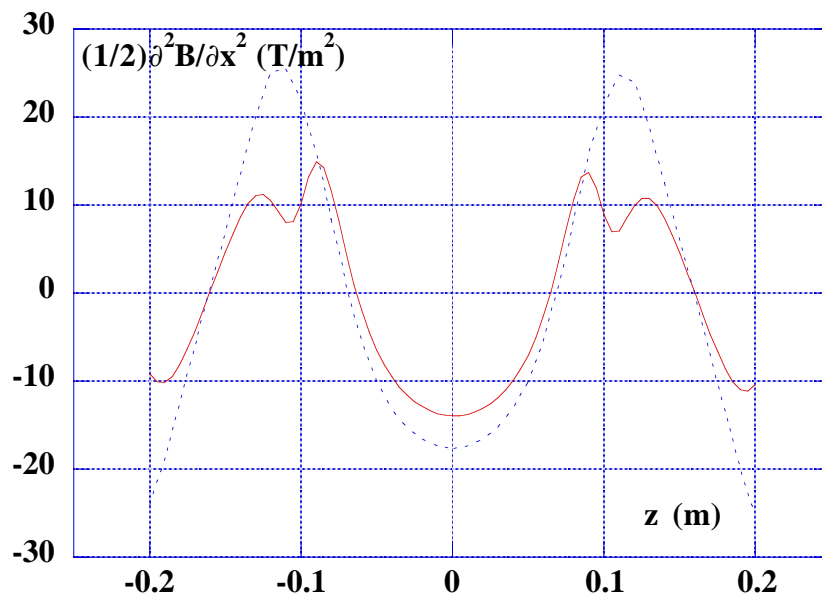
Fig. 19 - 2nd order term of 6th order transverse fit versus longitudinal position.
full line = second profile; dotted line = first profile.

6. Reduction of the gap

All the modifications described in the preceding Sections led to a reduction of ≈11% in the peak wiggler field. A careful check of the wiggler geometry with the vacuum chamber in the DAΦNE

Main Rings showed that it is possible to reduce the gap from the original value of 40 mm down to 37 mm. The separators between the two halves of the C-shaped supports were therefore machined to reduce their thickness from 28 mm to 25 mm. Figure 20 shows the difference in the field in the center pole with respect to the "second profile" configuration. The gain is $\approx 3\%$, while no significant variations appear in the higher order terms.
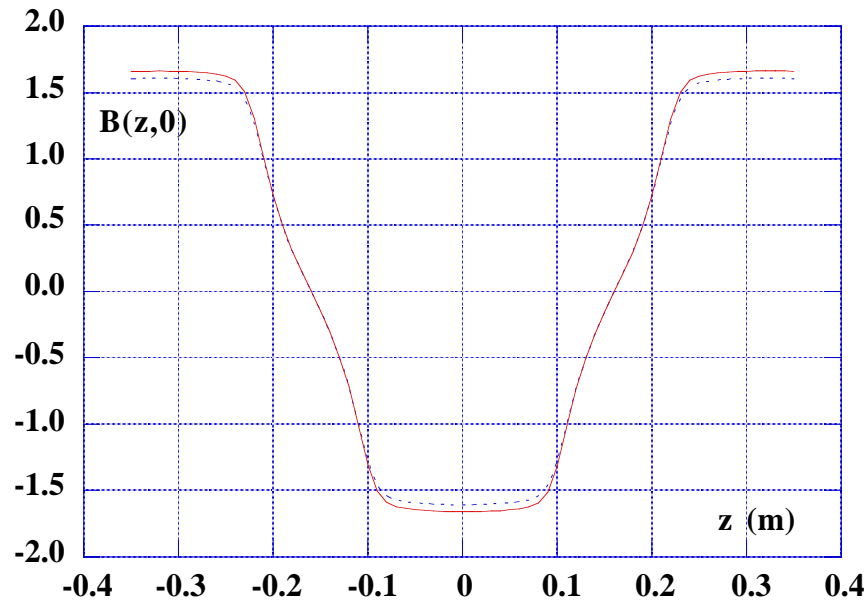
Fig. 20 - 0th order term of 6th order transverse fit versus longitudinal position.
full line = second profile gap=37 mm; dotted line = second profile gap = 40 mm.

7. Sextupole term in the terminal pole

From the study of non linear beam dynamics it was realized that a rather strong horizontally focusing sextupole in the terminal pole of the wiggler on the side of the quadrupole doublet could substantially improve the dynamic aperture of the ring. The required sextupole term corresponds to a value of K_{MAD} of ≈ 5 m^{-3}. The shape of pole surface has been designed with the criterion described in Section 4 and is shown in Fig. 21.
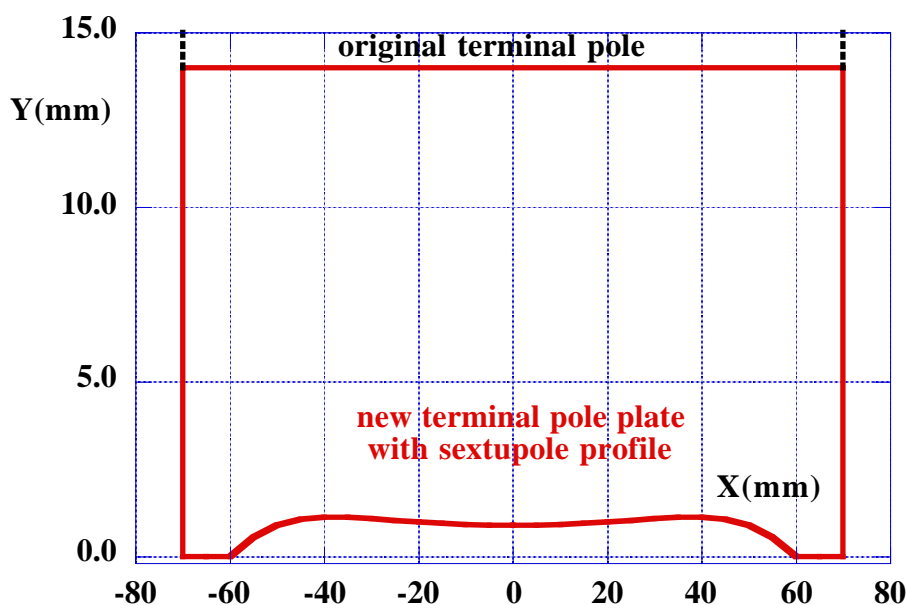
Fig. 21 - Plate shape of terminal pole with sextupole term superimposed (not in scale).

The field below the pole has been measured and fitted with a fourth order polynomial. The resulting second derivative of the field as a function of longitudinal position is shown in Fig. 22, compared to the same quantity in the flat pole configuration.
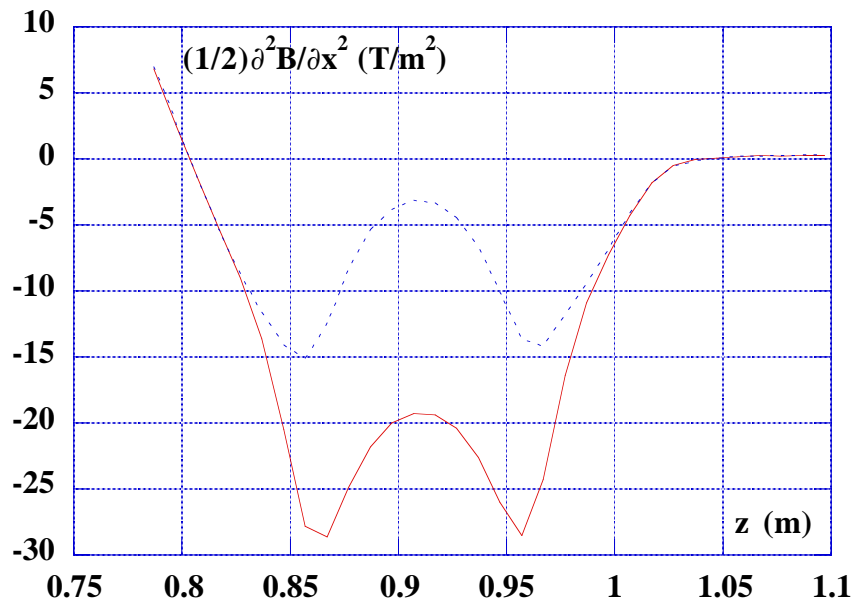
Fig. 22 - 2nd order term of 4th order polynomial fit versus longitudinal position in terminal pole.
full line = sextupole profile; dotted line = flat pole.

The value of the sextupole constant changes from 2.0 m^{-2} to 4.4 m^{-2}. The fourth order term also changes significantly, and is shown in Fig. 23.
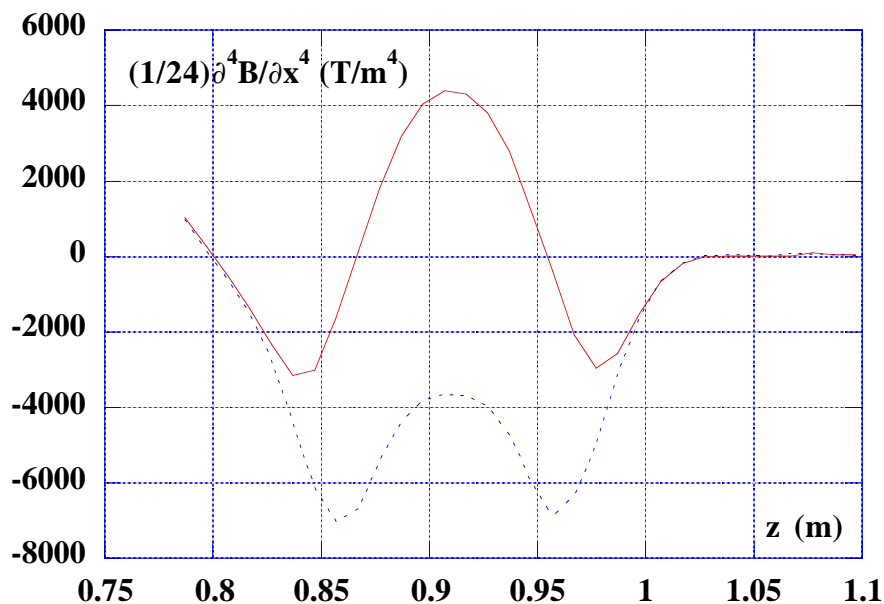
Fig. 23 - 4th order term of 4th order polynomial fit versus longitudinal position in terminal pole.
full line = sextupole profile; dotted line = flat pole.

8. Final configuration

In order to further gain in maximum field it was decided to reduce the maximum thickness of the plates from the original 14 mm to 7 mm and correspondingly the thickness of the separators between the C-shaped supports from 25 mm to 11 mm. Figure 24 shows the comparison between the field in the central pole in this final configuration and that in the original wiggler described in Section 2.
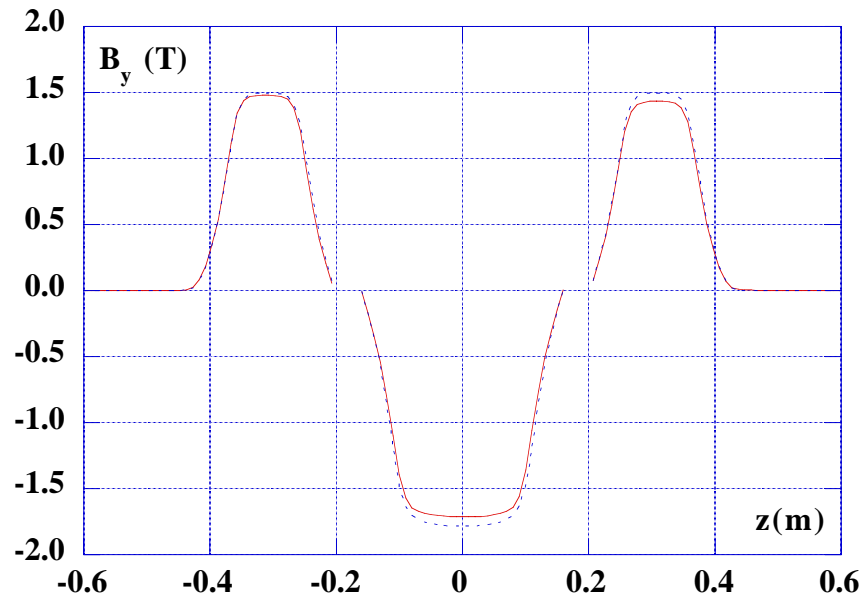
Fig. 24 - Vertical field component in central and terminal poles.
full line =final configuration; dotted line = original configuration

The maximum field in the central pole is smaller by 4%. The same factor holds for the terminal pole without the additional sextupole profile described in Section 7 (from here on called terminal A), while the other one (terminal B, on the left in Fig. 24), due to its different shape, is only 1% weaker than in the original configuration. This difference between the two terminal poles introduces an asymmetry in the wiggler field which is expected to produce a displacement between the position of the beam at the entrance and exit points even with a perfectly compensated field configuration obtained by changing the current in the terminal poles until a vanishing field integral on the trajectory is obtained.

We tried therefore to minimize this harmful effect by changing the position of the field clamp on terminal A. Increasing the distance of the clamps from the wiggler axis has the effect of increasing the field in the nearby terminal pole. In the normal configuration of the wiggler with both clamps at the same distance of 37 mm as in the poles, the measured field integral in terminal B at 564 A was 0.210 Tm, while the corresponding value in terminal A was 0.204 Tm. Since the clamp is fixed to the magnet yoke by means of four bolts, we could measure a second configuration with the gap in the clamp at 290 mm by using the lower hole in the clamp and the upper one in the yoke. A third point, although very near to the first one, was obtained by removing the 7 mm thick plates glued on the clamp in order to make the gap constant over the whole wiggler. Since the field integral in terminal B changes slightly when the position of the clamp in terminal A is changed, the distance where the two integrals are the same has been obtained from the crossing of the two straight lines through the measured points, as shown in Fig. 25 corresponding to a gap of 111 mm. The behaviour of the higher order terms is shown for the whole magnet in the next Section.
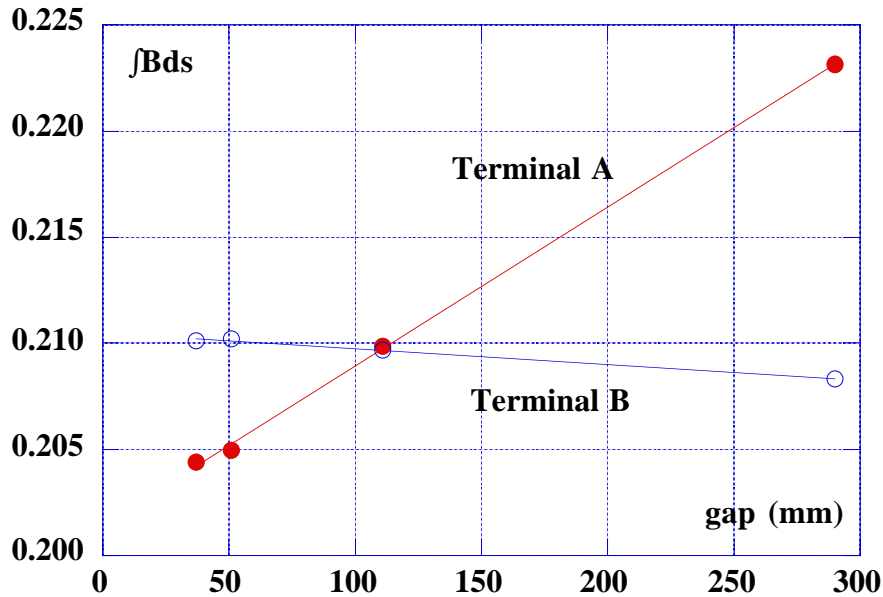
Fig. 25 - Field integral in terminal poles versus gap in the field clamp on terminal A.

All wigglers in DAΦNE have been modified to this final configuration at the end oh the 2003 shutdown for the installation of the FINUDA detector, including the modification of the clamp gap in terminal A.

9. Measurements with the double probe system

In fall 2003 the Hall probe positioning system [3] was equipped with a new T-shaped support capable of holding two probes at such a distance that any point inside the wiggler could be measured by at least one of the two probes. The mechanical distance between the two probes was set at 267.0 mm in such a way that after 30 steps of 8.9 mm the points covered by the first probe could be measured by the second one. Unfortunately, it has not been possible to intercalibrate the two probes. A plot of the difference between the two measurements in the region where the two probes can reach the same position is shown in Fig. 26.
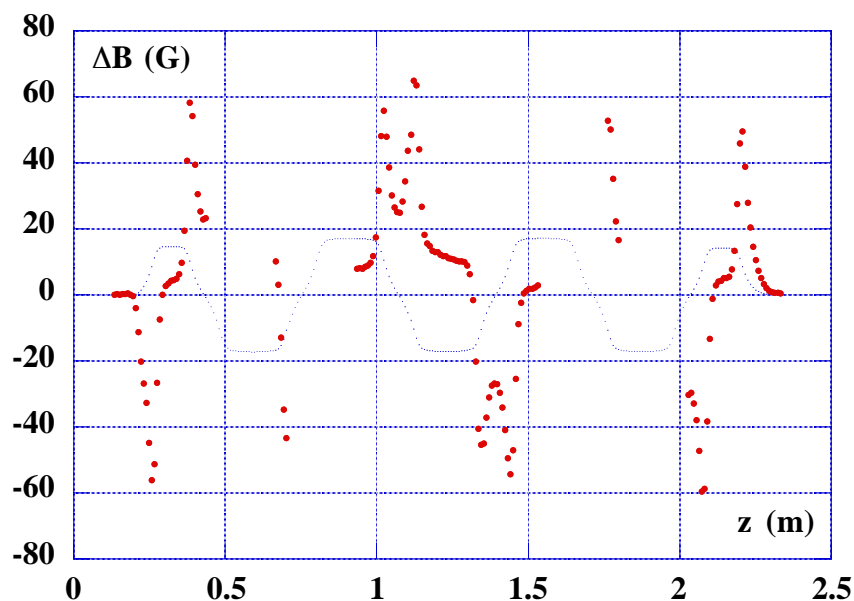
Fig. 26 - Difference between the two Hall probes at the same position (big dots, G)
and average field (small dots, KG)

It is clear that the difference can come both from a miscalibration between the two probes and from an error in the relative positioning on the same point. In particular, the maximum slope of the field at the transition between two adjacent poles is ≈150 G/mm. As shown in Fig. 26 the maximum deviations occur where the slope of the field is strong, while the difference tends to be small and flat around the flat tops of the field at the center of the poles. The deviation ranges between ±60 G. We tried therefore to measure the relative distance between the sensitive regions of the probes by setting the position of the first probe in a point of vanishing field between two poles, and then moving the second one until the same value of the field was reached. The measurement yielded a displacement of 267.2 mm. The step was therefore modified to 8.35 mm, requiring 32 steps to reach the same position. The maximum difference between the probes dropped by a factor ≈3, as shown in Fig. 27.
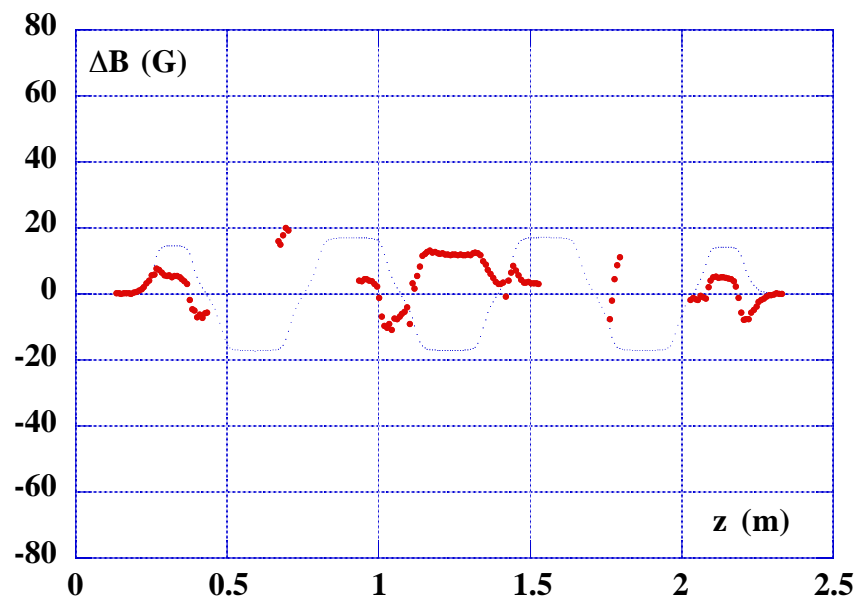
*Fig. 27 - Difference between the two Hall probes at the same position (big dots)
and average field (small dots, KG) after changing the step to 8.35 mm*

In the absence of an intercalibration of the two probes we decided to take as field value the measurement from one probe at those positions where the other one could not be placed and the average where both measurements can be performed.

With the currents used for the measurement of the wiggler in its original configuration (693A in the full poles and 564 A in the terminal ones) the field integral on axis was found to be 70.5 Gm. We repeated the measurement changing the current in the terminal poles until the field integral on axis was below 1 Gm, finding the optimum current at 486A. However, the condition of vanishing field integral had still to be verified on the wiggling trajectory rather than on axis. For this reason the final characterization of the wiggler field required the measurement of the vertical field component on the wiggler symmetry plane.

A full map consisting of 328 longitudinal positions spaced by 8.35 mm and 15 transverse ones spaced by 10 mm (4920 points) was measured in a single run of ≈7 hours in December 2003.

10. Calculation of the beam trajectory

The measurement of the full map was used to find out the properties of the beam trajectory inside the wiggler and the first order transfer matrix of the magnet. The method of integration is described in [4]. Since the nominal trajectory in the wiggler oscillates with respect to the magnet axis with an amplitude of ≈12 mm, the dependence of the vertical field component on the transverse displacement is approximated with a second order polynomial fitting the measured field points between ±30 mm from the axis, while the longitudinal dependence is interpolated with a fourth order polynomial. The result does not change if the field is fitted with a fourth order polynomial, and this is useful to evaluate higher order components in the field (see next Section). Figure 28 shows the result of the

integration for a particle starting outside the wiggler field at a distance of 11.8 mm from the wiggler axis and parallel to it. Both cases of start from the side of terminal A and terminal B are considered.
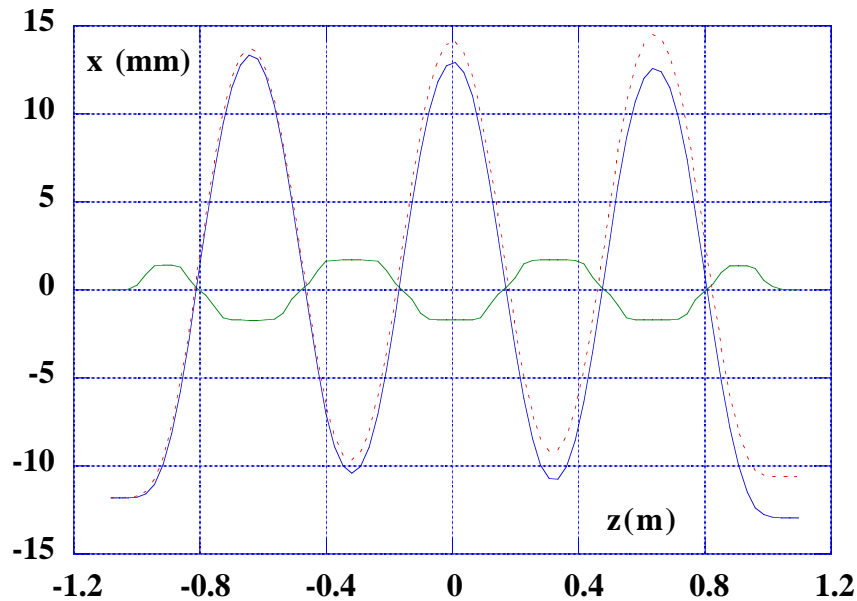
Fig. 28 - Horizontal beam trajectories in the wiggler starting at -11.8 mm parallel to the wiggler axis. Full line = start from terminal B, dotted line = start from terminal A. The field in Tesla is indicated for reference

As indicated in Section 8 there is a displacement between the entry and exit points of the trajectory of ≈1.2 mm, of opposite sign for the two cases, while the field integral on the trajectory does not differ from that calculated on the wiggler axis (less than 2 Gm), keeping the exit angle below 0.1 mrad.

As described in [4], the horizontal and longitudinal field components can be calculated from the map of the vertical one on the symmetry plane in its vicinity, and therefore also the motion of the particles in the vertical plane can be integrated. Figure 29 shows two typical trajectories, one starting parallel to the wiggler axis at a distance of 1 mm from it and second starting on the wiggler axis with an angle of 1 mrad. The vertical focusing effect of the wiggler is evident.
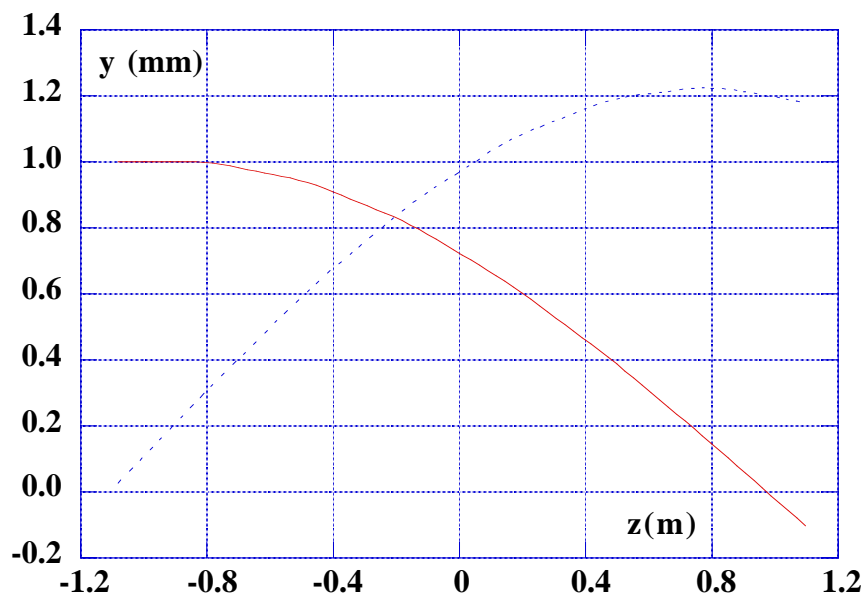
Fig. 29 - Vertical beam trajectories in the wiggler starting at 1 mm parallel to the wiggler axis (full line) and on axis with an angle of 1 mrad (dotted line)

By calculating the beam trajectories as a function of small changes in the initial conditions of horizontal and vertical position and angle and in the beam energy it is possible to calculate the wiggler transfer matrix [4]. For the case where the beam starts from the side of terminal B we find:

$$
\mathbf{M_{B\text{->}A}} = \begin{pmatrix}
1.13395 & 2.28576 & 0.00031 & 0.00767 & -0.00044 \\
0.07580 & 1.03514 & -0.00049 & 0.00360 & -0.00052 \\
0 & 0 & 1 & 0 & 0 \\
0 & 0 & 0 & -0.18381 & 1.17653 \\
0 & 0 & 0 & -0.83261 & -0.11092
\end{pmatrix}
$$

It is possible to observe that the contribution to the dispersion is very small, as well as the coupling terms arising from the beam displacement in the vertical plane.

In the case where the beam starts from terminal A we find the following matrix, where in the ideal case we should find element m(1,1) equal to m(2,2) of the first one and the other way round, as well as for m(4,4) and m(5,5). We attribute the small difference to the different field seen by the particles following the slightly different trajectories shown in Fig. 28.

$$
\mathbf{M_{A\text{->}B}} = \begin{pmatrix}
1.03489 & 2.28369 & -0.00149 & -0.00044 & 0.00030 \\
0.07202 & 1.12119 & -0.00068 & -0.00035 & 0.00501 \\
0 & 0 & 1 & 0 & 0 \\
0 & 0 & 0 & -0.11151 & 1.17685 \\
0 & 0 & 0 & -0.83276 & -0.17886
\end{pmatrix}
$$

11. Calculation of the higher order terms

As explained in the introduction the different terms in the field transverse expansion have effects on the beam dynamics which can be summarized by the constants K_{MAD} which can now be calculated on the wiggling trajectory starting from the knowledge of the trajectory and of the field derivatives on the wiggler axis. Since we are interested mainly in the field properties for stable particles, and in particular to the tune shift effect described in the introduction, we restrict, for the moment, our analysis to the expansion of the field up to the fourth order and the horizontal range between ±40 mm, as explained in Sections 2 and 4. The following Figs. 30,31,32,33,34 show the behaviour of the 5 terms of the fourth order polynomial fitting the transverse behaviour of the field as a function of longitudinal position. An explanation for the anomalous peak observed in the third order term corresponding to the second full pole has not yet been found. However the contribution of this term to the transverse variation of the field at the typical distance of 1 cm is negligible with respect to the leading second order term.
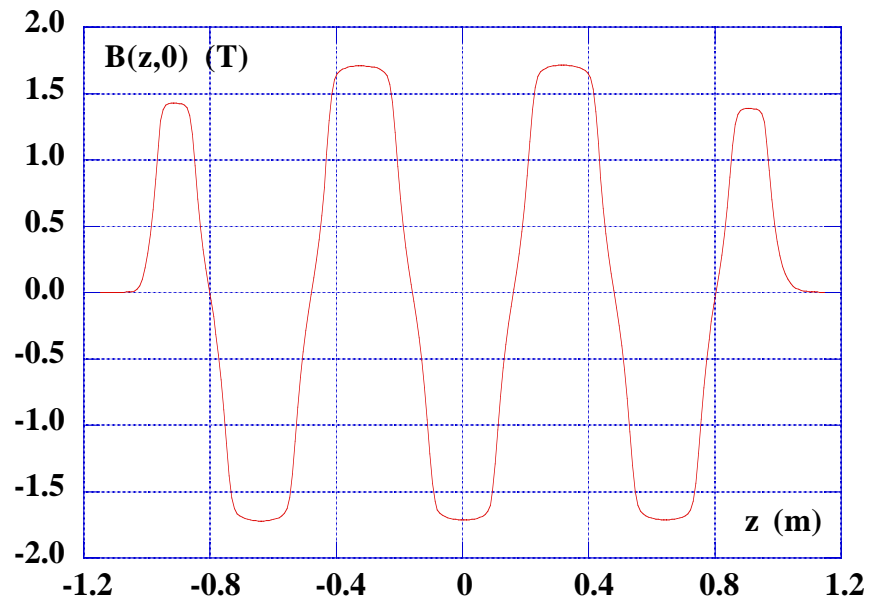
Fig. 30 - 0th order term of transverse expansion with a fourth order polynomial
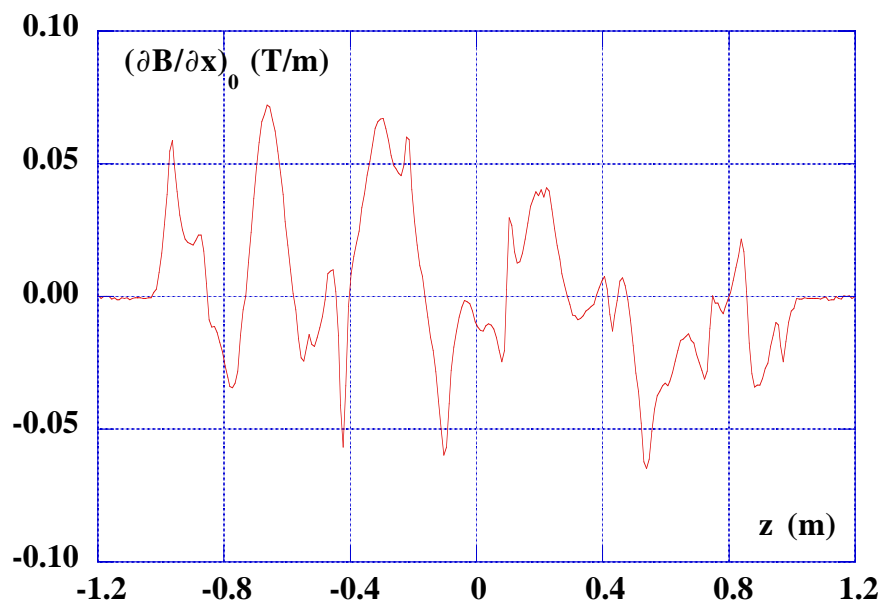
Fig. 31 - First order term of transverse expansion with a fourth order polynomial
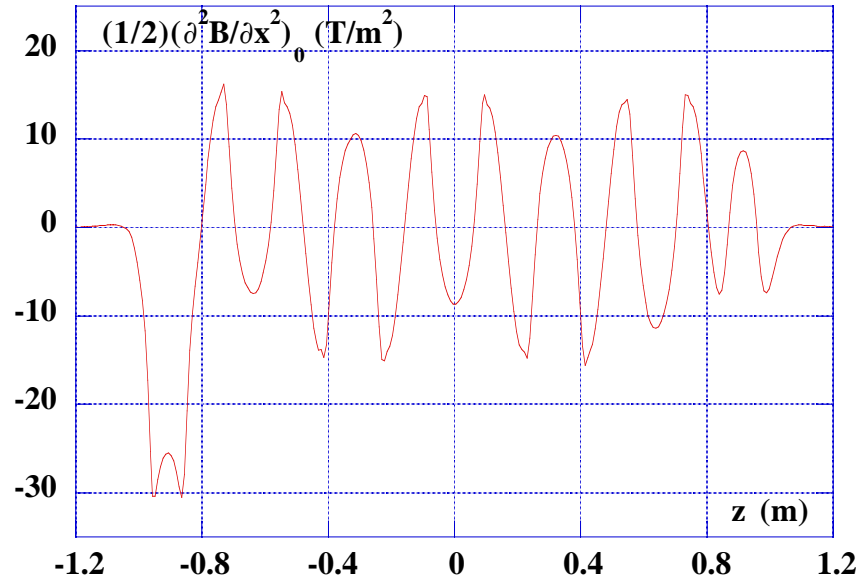
Fig. 32 - Second order term of transverse expansion with a fourth order polynomial
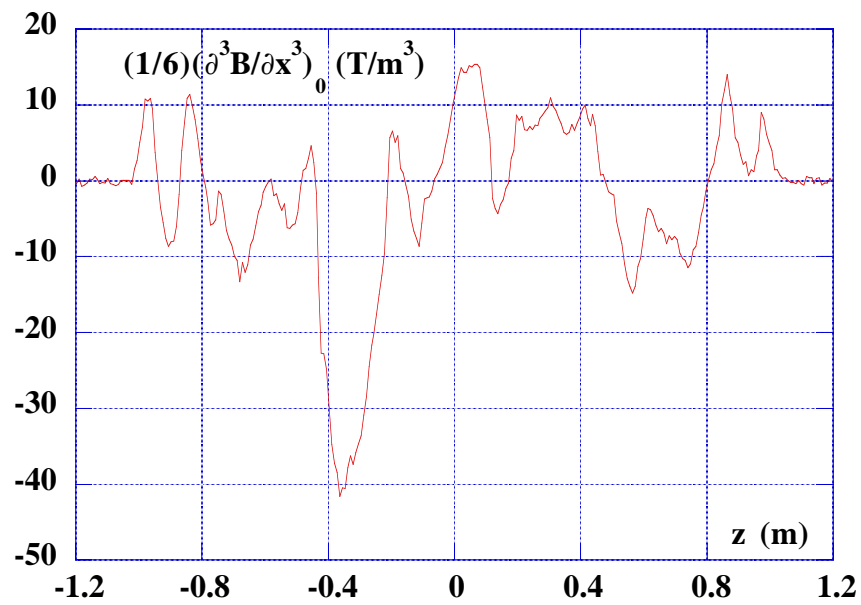
Fig. 33 - Third order term of transverse expansion with a fourth order polynomial
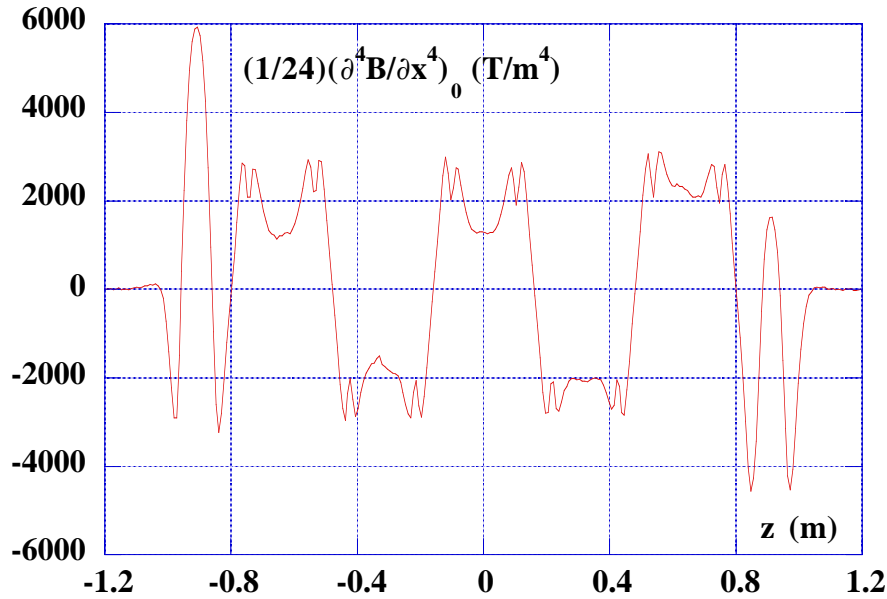
Fig. 34 - Fourth order term of transverse expansion with a fourth order polynomial

We can combine the terms of the transverse expansion to find the contributions to K_{MAD} defined in Section 1. We recall here the explicit expressions, where all derivatives are taken on the wiggler axis. Table I collects all the contributions.

$$K_1^{MAD} = \frac{1}{B\rho}\left[\int \frac{\partial B}{\partial x}\,dz + \int \frac{\partial^2 B}{\partial x^2}\,x\,dz + \frac{1}{2}\int \frac{\partial^3 B}{\partial x^3}\,x^2\,dz + \frac{1}{6}\int \frac{\partial^4 B}{\partial x^4}\,x^3\,dz\right]$$

$$K_2^{MAD} = \frac{1}{B\rho}\left[\int \frac{\partial^2 B}{\partial x^2}\,dz + \int \frac{\partial^3 B}{\partial x^3}\,x\,dz + \frac{1}{2}\int \frac{\partial^4 B}{\partial x^4}\,x^2\,dz\right]$$

$$K_3^{MAD} = \frac{1}{B\rho}\left[\int \frac{\partial^3 B}{\partial x^3}\,dz + \int \frac{\partial^4 B}{\partial x^4}\,x\,dz\right]$$

$$K_4^{MAD} = \frac{1}{B\rho}\int \frac{\partial^4 B}{\partial x^4}\,dz$$

TABLE I - Contributions to K^{MAD} (the symbol E indicates an exponent of 10) obtained from 4th order polynomial fit. The fit ranges from -40 mm to +40 mm

	Term.B	First pole	Second pole	Third pole	Fourth pole	Fifth pole	Term.A	Full wiggler
$(1/B\rho)\int(\partial B/\partial x)dz$	0.002	0.002	0.005	-0.002	0.002	-0.005	-0.001	0.003
$(1/B\rho)\int(\partial^2 B/\partial x^2)x\,dz$	0.041	0.008	-0.001	0.005	1.6E-4	5.4E-4	5.7E-4	.055
$(1/2B\rho)\int(\partial^3 B/\partial x^3)x^2 dz$	6.8E-5	-3.3E-4	-8.7E-4	3.9E-4	2.6E-4	-3.9E-4	1.7E-4	-7.1E-4
$(1/6B\rho)\int(\partial^4 B/\partial x^4)x^3 dz$	4.2E-4	0.001	6.6E-4	0.001	8.3E-4	0.002	8.7E-4	.007
K_1^{MAD} (m^{-1})	0.043	0.012	0.004	0.005	0.003	-0.003	0.000	0.064
$(1/B\rho)\int(\partial^2 B/\partial x^2)\,dz$	-4.8	1.6	-1.1	1.4	-1.2	1.0	-0.2	-3.2
$(1/B\rho)\int(\partial^3 B/\partial x^3)x\,dz$	-0.01	-0.06	0.19	0.06	-0.06	-0.08	-0.03	0.01
$(1/2B\rho)\int(\partial^4 B/\partial x^4)x^2 dz$	0.15	0.39	-0.23	0.36	-0.27	0.47	-0.22	0.64
K_2^{MAD} (m^{-2})	-4.7	2.0	-1.1	1.8	-1.5	1.4	-0.4	-2.6
$(1/B\rho)\int(\partial^3 B/\partial x^3)\,dz$	2	-6	-21	5	8	-8	4	-17
$(1/B\rho)\int(\partial^4 B/\partial x^4)x\,dz$	-32	76	59	73	66	92	41	375
K_3^{MAD} (m^{-3})	-30	70	38	78	74	84	45	358
K_4^{MAD} (m^{-4})	2.8E3	8.3E3	-9.1E3	8.3E3	-9.4E3	10.0E3	-5.0E3	5.8E3

From the numbers shown in Table I we can draw the following conclusions:

- the "intrinsic" quadrupole term of the wiggler coming from gradient terms in the field and from the combination of the second and fourth order terms of the transverse expansion with the wiggling trajectory inside the wiggler is negligible everywhere, but in Terminal B, where the large displacement due to the entrance of the beam at $\approx$12 mm from the wiggler axis finds a large sextupole term. This "intrinsic" term does not include the vertical focusing due to the angle between the beam trajectory and the endcaps of the poles;

- the contribution to the sextupole term comes mainly from the second derivative of the field, and it is particularly large in Terminal B, where it has been enhanced, as explained in Section 7. The contribution from the fourth derivative is small, although not negligible;

- the octupole term determining the tune shift versus beam displacement in the wiggler described in the Introduction is due mainly to the combination of the fourth order term in the field with the wiggling trajectory and has been decreased by more than a factor 2. The difference in the sign comes from the arbitrary relative sign between the field and the trajectory. The amount of the reduction of this term on the tune shift versus beam displacement has been confirmed by preliminary measurements on DAΦNE;

- the influence of the decapole term on the particle motion is an order of magnitude smaller than the octupole at the typical oscillation amplitudes of the particles in the ring ($\approx$5 σ_x at 1 cm).

12. Behaviour of the field at large amplitudes

The fourth order polynomial fit used to obtain the results given in Section 11 is accurate in a limited range (between $\pm$40 mm) around the wiggler axis. Figure 35 shows the average discrepancy between the fit and the 9 points at the same longitudinal position. The discrepancy is always smaller than 2 G.
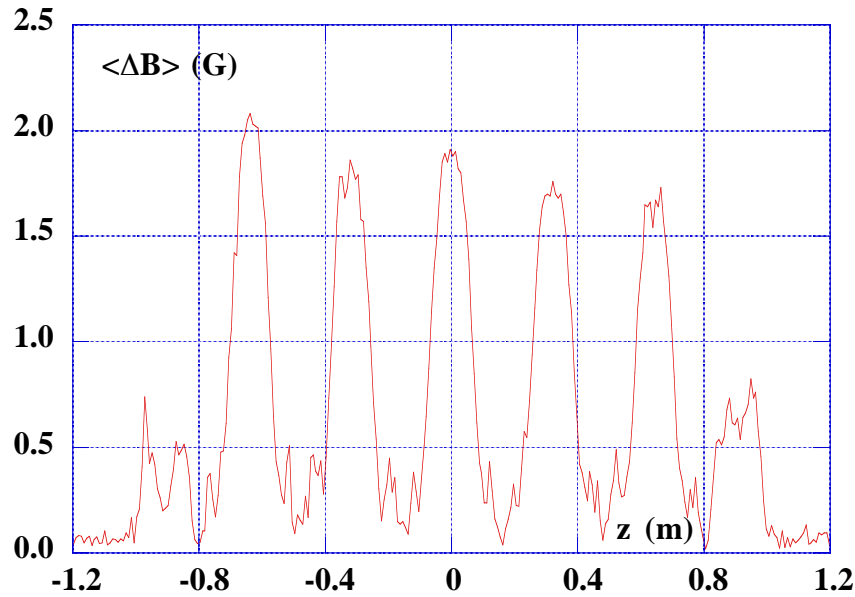
Fig. 35 - Average discrepancy between measured field and fourth order polynomial fit in the range between ±40 mm with respect to the wiggler axis.

The situation changes when we want to fit the measured field at larger amplitudes, which can be useful, for instance, to evaluate dynamic aperture and beam lifetime. As explained in Section 2, and due to the particular shape of the modified poles (see Fig. 11), we have tried to fit the transverse behaviour between ±60 mm with a particular polynomial of the sixth order without the third, fourth and fifth order terms, as explained in Section 2. This to avoid that the fitting function could present large terms of different sign cancelling each other.

Figure 36 shows the behaviour of the second order term, compared to that obtained with the fourth order polynomial fit between ±40 mm. The difference is not negligible and this indicates that some caution has to be taken when using these data for beam dynamics calculations. For the evaluation of beam properties at small oscillation amplitudes (within few standard deviations in the horizontal distribution) the data given in Table I are accurate. For larger amplitudes it is better to use the data obtained with the sixth order fit given in Table II.
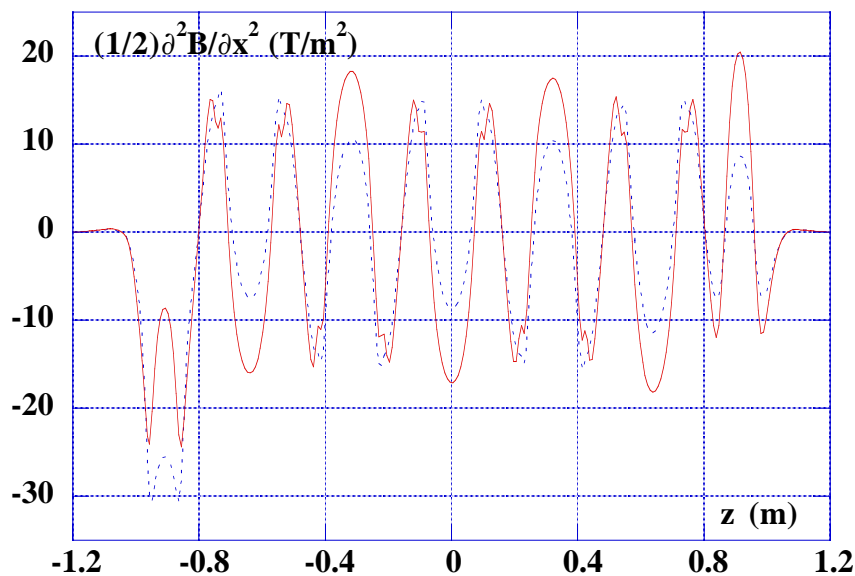
Fig. 36 - Second order term of sixth order fit (full line) between ±60 mm compared to the same term in the fourth order polynomial (dotted line) between ±40 mm, versus longitudinal position

Figure 37 shows the behaviour of the sixth order term, while Fig. 38 gives the average discrepancy between the measured points and the fit. Clearly this discrepancy is now much larger, up to 40 G.
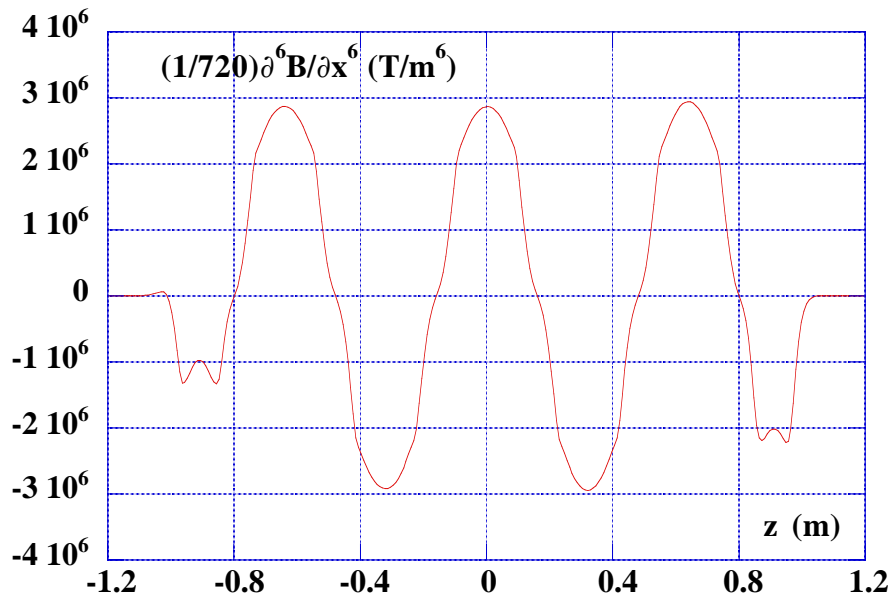
Fig. 37 - Sixth order term of sixth order fit along the wiggler between ±60 mm versus longitudinal position
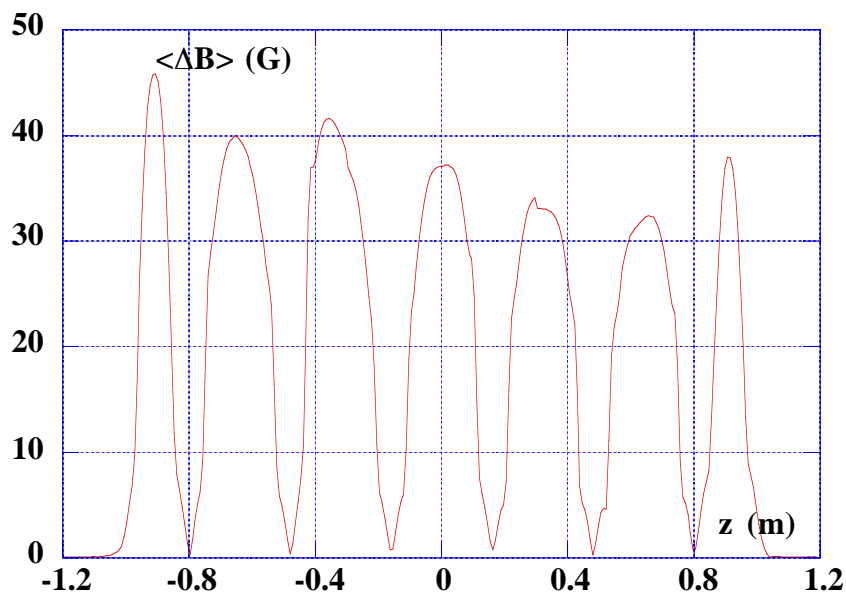
Fig. 38 - Average discrepancy between measured field and sixth order fit in the range between ±60 mm with respect to the wiggler axis.

The contributions to the values of K_{MAD} using the sixth order fit must now be calculated up to the sixth order. We have:

$$K_1^{MAD} = \frac{1}{B\rho}\left[\int \frac{\partial B}{\partial x}dz + \int \frac{\partial^2 B}{\partial x^2}xdz + \frac{1}{120}\int \frac{\partial^6 B}{\partial x^6}x^5dz\right]$$

$$K_2^{MAD} = \frac{1}{B\rho}\left[\int \frac{\partial^2 B}{\partial x^2}dz + \frac{1}{24}\int \frac{\partial^6 B}{\partial x^6}x^4dz\right]$$

$$K_3^{MAD} = \frac{1}{6B\rho}\int \frac{\partial^6 B}{\partial x^6}x^3dz$$

$$K_4^{MAD} = \frac{1}{2B\rho}\int \frac{\partial^6 B}{\partial x^6}x^2dz$$

$$K_5^{MAD} = \frac{1}{B\rho}\int \frac{\partial^6 B}{\partial x^6}xdz$$

$$K_6^{MAD} = \frac{1}{B\rho}\int \frac{\partial^6 B}{\partial x^6}dz$$

Table II collects the contributions of the different terms.

TABLE II - Contributions to K^{MAD} (the symbol E indicates an exponent of 10) obtained from 6th order fit. The fit ranges form -60 mm to +60 mm.

	Term.B	First pole	Second pole	Third pole	Fourth pole	Fifth pole	Term.A	Full wiggler
$(1/B\rho)\int(\partial B/\partial x)dz$	0.007	-0.009	0.010	-0.010	0.011	-0.014	0.003	-0.002
$(1/B\rho)\int(\partial^2 B/\partial x^2)x\,dz$	0.028	-0.009	-0.014	-0.012	-0.012	-0.014	-0.006	-0.039
$(1/120B\rho)\int(\partial^6 B/\partial x^6)x^5dz$	5.8E-5	4.8E-4	1.3E-4	3.9E-4	1.7E-4	3.1E-4	1.9E4	0.002
K_1^{MAD} (m^{-1})	0.034	-0.017	-0.004	-0.022	-0.001	-0.027	-0.003	-0.040
$(1/B\rho)\int(\partial^2 B/\partial x^2)\,dz$	-3.4	0.26	0.18	-0.034	0.049	-0.082	0.43	-2.6
$(1/24B\rho)\int(\partial^6 B/\partial x^6)x^4dz$	-0.027	0.19	-0.067	0.16	-0.086	0.14	-0.079	0.23
K_2^{MAD} (m^{-2})	-3.43	0.46	0.12	0.13	0.0	0.05	0.35	-2.3
K_3^{MAD} (m^{-3})	10	64	28	56	34	49	27	268
K_4^{MAD} (m^{-4})	-3.1E3	1.6E4	-9.2E3	1.5E4	-1.1E4	1.4E4	-7.1E3	1.5E4
K_5^{MAD} (m^{-5})	6.5E5	2.8E6	2.1E6	2.7E6	2.2E6	2.6E6	1.3E6	1.4E7
K_6^{MAD} (m^{-6})	-7.82E7	2.56E8	-2.59E8	2.56E8	-2.58E8	2.59E8	-1.32E8	4.4E7

13. Conclusions

An additional wiggler, built by on the same design and with the same materials of the wigglers installed on DAΦNE. has been purchased by LNF with the aim of reducing the effect of field distorsions on the beam dynamics.

The shape of the poles has been modified by glueing additional profiled iron plates on the poles. Magnetic measurements have been performed in order to increase the flat field region around the wiggler axis and to widen the distance between the two rapid fall-offs of the field near the pole boundaries.

Particle tracking inside the measured field has been used to determine the correct compensation currents, to find the transfer matrix of the wiggler and to establish the contributions of high order terms in the field to the non-linear particle dynamics. Significant reduction of the sextupole and octupole effects in the wiggler has been achieved. This has been verified by preliminary measurements such as those described in the Introduction, showing a reduction by a factor ≈ 2.5 in the intensity of the octupole contribution from the wiggler. More precise measurements will be performed early this year. All wigglers in DAΦNE have been modified to the final configuration described in Section 8.

References

[1] B. Bolli, F. Iungo, M. Modena, M. Preger, C. Sanelli, F. Sgamma, S. Vescovi: "Measurements on the wiggler magnet for the DAΦNE Main Rings" DAΦNE Technical Note M-4 (28/4/1994).

[2] B. Bolli, N. Ganlin, F. Iungo, F. Losciale, M. Preger, C. Sanelli, F. Sardone: "Magnetic measurements on the series production wigglers of the DAΦNE achromats" DAΦNE Technical Note MM-29 (30/6/1997).

[3] B. Bolli, N. Ganlin, F. Iungo, F. Losciale, M. Paris, M. Preger, C. Sanelli, F. Sardone, F. Sgamma, M. Troiani: "The dipoles of the DAΦNE achromats" DAΦNE Technical Note MM-26 (22/5/1997).

[4] M. Preger: "The wiggler transfer matrix" DAΦNE Technical Note L-34 (18/11/2003).